PHYSICAL REVIEW D **85,** 014009 (2012)

Spontaneous *CP* violation in quark scattering from QCD *Z*(3) interfaces

Abhishek Atreya* and Ajit M. Srivastava†
Institute of Physics, Bhubaneswar, 751005, India

Anjishnu Sarkar‡
Physical Research Laboratory, Ahmedabad, 380009, India

(Received 5 August 2011; revised manuscript received 13 November 2011; published 11 January 2012)

In this paper, we explore the possibility of spontaneous *CP* violation in the scattering of quarks and antiquarks from QCD *Z*(3) domain walls. The *CP* violation here arises from the nontrivial profile of the background gauge field (A_0) between different *Z*(3) vacua. We calculate the spatial variation of A_0 across the Z(3) interface from the profile of the Polyakov loop $L(\vec{x})$ for the Z(3) interface and calculate the reflection of quarks and antiquarks using the Dirac equation. This spontaneous *CP* violation has interesting consequences for the relativistic heavy-ion collision experiments, such as baryon enhancement at high P_T. It also acts as a source of additional J/ψ suppression. We also discuss its implications for the early Universe.

DOI: 10.1103/PhysRevD.85.014009 PACS numbers: 25.75.−q, 11.27.+d, 12.38.Mh

I. INTRODUCTION

The possibility of extended topological objects in the quark-gluon plasma (QGP) phase, e.g. Z(3) interfaces arising from spontaneous breaking of Z(3) symmetry, has been extensively discussed in the literature [1–3]. It has also been pointed out that there are also topological string defects in QGP forming at the junctions of Z(3) walls [4]. Formation and evolution of these objects in the initial transition to the QGP phase has been studied in the context of relativistic heavy-ion collision experiments (RHICE) [5]. Certain consequences of Z(3) walls for baryon inhomogeneity generation in the Universe have also been explored [6]. Investigation of these objects is important not only for probing the very rich vacuum structure of the QCD in the deconfining phase, but also because these provide the only example of topological defects in a relativistic quantum field theory which can be probed in laboratory conditions, namely, RHICE. The existence of these objects has been questioned in the literature, especially in the presence of quarks [7,8]. However, there are recent lattice studies by Deka *et al.* [9] of QCD with quarks which have attempted to directly probe the existence of different Z(3) vacua. These results show a strong possibility of the existence of nontrivial, metastable, Z(3) vacua for high temperatures. The exact value of the temperature, above which these metastable Z(3) vacua are seen, is not important. What is important is that these vacua seem to exist as metastable thermodynamic phases of QCD in the deconfining regime, and hence associated topological objects will necessarily arise in any realistic phase transition from the confining phase to the QGP phase.

In this paper we will investigate an interesting possibility arising from the existence of Z(3) interfaces. We will study the reflection of quarks and antiquarks from Z(3) walls and show the existence of *CP* violation arising from the Z(3) walls. This *CP* violation is spontaneous, arising due to the background configuration of the gauge field corresponding to the Z(3) wall, and was first demonstrated by Korthals Altes *et al.* [10]. It was shown in Ref. [10], in the context of the Universe, that due to the nontrivial background field configuration for the standard model gauge fields, the localization of quarks and antiquarks on the wall is different. Its possible effects on the electroweak baryogenesis via sphalerons was discussed in [10]. The same possibility of spontaneous *CP* violation for the case of QCD was also discussed in [11]. We extend these studies by calculating the propagation of quarks and antiquarks across the Z(3) walls and show that they have different reflection coefficients. For this we calculate the profile of the order parameter $L(\vec{x})$ between different Z(3) vacua [4] using the effective potential for the Polyakov loop, as proposed by Pisarski [12]. We then obtain the profile of the background gauge field A_0 from this $L(\vec{x})$ profile. This A_0 configuration provides a potential for the propagation of quark causing nontrivial reflection of quarks from the wall. It is important to know the uncertainties in the determination of the A_0 profile depending on the choice of the specific form of the effective potential, such as those given in [13,14]. To address this issue we repeat the above calculation for another choice of effective potential of the Polyakov loop as provided by Fukushima [13]. We find that, even though the two effective potentials (in Refs. [12,13]) are of qualitatively different shapes, the resulting wall profile and A_0 profile are surprisingly similar. This gives us confidence in the use of our procedure to calculate the reflection of quark and antiquarks from the Z(3) interfaces.

*atreya@iopb.res.in
†ajit@iopb.res.in
‡anjishnu@prl.res.in

Different values of the reflection coefficients of quarks and antiquarks from the Z(3) walls will have very interesting implications for the case of RHICE and for the early Universe. Here we mention that in the earlier studies by some of us the reflection of quarks/antiquarks from Z(3) walls (in the context of RHICE and the Universe) [6], was studied by modeling the dependence of effective quark mass on the magnitude of the Polyakov loop, and no possibility of spontaneous *CP* violation was explored. This *CP* violation, resulting in different reflection coefficients of quarks and antiquarks from Z(3) walls, will lead to segregation of quarks and antiquarks due to motion (collapse) of walls. As a result there will be selective concentration of baryon (or antibaryon) number in different regions, depending on the Z(3) vacua involved. This will have direct observable consequences for the relativistic heavy-ion collision experiments. For example, it will affect the yield of baryons and mesons, enhancing baryon multiplicities and suppressing meson multiplicities. As we will see, these effects are expected to be important for heavy quarks, especially for charm and heavier flavors. A detailed analysis of these effects is planned for a future work. This *CP* violation can also play an important role in the context of the early Universe, especially for generation of baryon density inhomogeneities, by segregating baryons and antibaryons. We mention here that our analysis of the reflection of quarks in this paper utilizes Z(3) wall profile of pure SU(3) gauge theory, without dynamical quarks. The effects of quarks may not be important in the context of RHICE due to small length and time scales involved, but for the case of the Universe these effects will be of crucial importance. We will discuss this further below.

The paper is organized in the following manner. In Sec. II, we discus the basic physics of the origin of spontaneous *CP* violation due to the presence of Z(3) interfaces [10,11] and discuss the effective potential for the Polyakov loop, as proposed by Pisarski [12] for calculating various quantities. In Sec. III, we discuss how to obtain the profile of the background gauge field A_0 from the profile of the order parameter $L(\vec{x})$ between different Z(3) vacua [4]. In Sec. IV, we address the issue of uncertainties in the determination of the A_0 profile depending on the choice of the specific form of the effective potential by repeating the calculations of Sec. III for the effective potential of the Polyakov loop provided by Fukushima [13]. The resulting wall profile and A_0 profile are found to be very close to those found in Sec. III. We use the profile of A_0 as calculated in Sec. III, for the Dirac equation (in the Minkowski space) in Sec. V to calculate the reflection and transmission coefficients for quarks and antiquarks. Section VI presents our results and conclusions are discussed in Sec. VII.

II. ORIGIN OF SPONTANEOUS *CP* VIOLATION

We first discuss the basic physics of the origin of the spontaneous *CP* violation from the existence of Z(3) walls. For the case of pure $SU(N)$ gauge theory, we start with the definition of the Polyakov loop, [15–17]

$$L(x) = \frac{1}{N}\,\mathrm{Tr}\left[\mathbf{P}\exp\left(ig\int_0^\beta A_0(\vec{x},\tau)d\tau\right)\right], \qquad (1)$$

where $A_0(\vec{x},\tau) = A_0^a(\vec{x},\tau)T^a$, $(a = 1,\ldots N)$ are the gauge fields and T^a are the generators of $SU(N)$ in the fundamental representation. $\mathbf{P}$ denotes the path ordering in the Euclidean time τ, and g is the gauge coupling. Under global $Z(N)$ symmetry transformation, the Polyakov Loop transforms as

$$L(x) \to Z \times L(x), \quad \text{where } Z = e^{i\phi}. \qquad (2)$$

Here, $\phi = 2\pi m/N$; $m = 0, 1\ldots(N-1)$.

The thermal average of the Polyakov loop, $\langle L(x)\rangle$, is the order parameter for the confinement-deconfinement phase transition. (From now onwards, we will use $L(x)$ to denote $\langle L(x)\rangle$.) It is related to the free energy of a test quark in a pure gluonic medium ($L(x) \propto e^{-\beta F}$). $L(x) \neq 0$ implies finite free energy of a test quark and hence, the deconfined phase (i.e. the system is above the critical temperature T_c). This leads to spontaneous breaking of $Z(N)$ symmetry. On the other hand, $L(\vec{x}) = 0$ implies infinite free energy of a test quark and hence, confined phase (i.e. the system is below T_c). The $Z(N)$ symmetry is then restored. The N-fold degeneracy of the ground state implies the existence of interfaces between regions of different $Z(3)$ vacua. For QCD, the gauge group is the color group $SU(3)_c$. It has three $Z(3)$ vacua resulting from the spontaneous breaking of $Z(3)$ symmetry in the high temperature (deconfined) phase characterized by

$$L(\vec{x}) = 1, e^{i2\pi/3}, e^{i4\pi/3}. \qquad (3)$$

As we mentioned above, there have been questions as to whether these Z(3) domains have some physical meaning or not [7,8]. The inclusion of quarks raises further issues as they do not respect the $Z(N)$ symmetry. It has been argued that it is possible to interpret the effect of addition of quarks as the explicit breaking of $Z(N)$ symmetry and lifting of degeneracy of the vacuum [12,18–20], and we will follow this approach. Further, as we mentioned in the Introduction, recent lattice QCD studies with quarks [9] have strengthened the physical basis for the existence of these different Z(3) vacua. The metastability of nontrivial $Z(3)$ vacua will have important implications for RHICE and the early Universe. However, in the remainder of the paper we will consider the pure gauge case for calculating the $Z(3)$ interface profiles. This is because our main objective here is to show the interesting possibility of spontaneous *CP* violation in the reflection of quarks and antiquarks from Z(3) walls which is independent of the explicit symmetry breaking. We will briefly comment on the effects of quarks in the last section, and detailed study of these effects will be presented in a future work.

As mentioned earlier, different $Z(3)$ vacua have an interpolating $L(\vec{x})$ profile leading to Z(3) interfaces. This essentially means that there is a background gauge field $A_0(\vec{x})$ profile which interpolates between different $Z(3)$ vacua. The quarks/antiquarks moving across the $Z(3)$ domain walls will behave differently in the presence of a given spatially varying A_0 field configuration. As a result, we should have different reflection and transmission coefficient for quarks and antiquarks. This is the source of *CP* violation. The origin of this *CP* asymmetry is spontaneous in nature. The earlier studies [10,11] of this spontaneous *CP* violation arising from Z(3) walls focused on the localized solution of the Dirac equation (in Euclidean space), and it was shown that if a wave function for a fermion species localizes, then its *CP* conjugate does not. The whole discussion in Refs. [10,11] was within the Euclidean formalism and the exact gauge field profile was not determined in these investigations.

In this paper we are interested in the calculation of reflection and transmission coefficient of quarks and antiquarks and hence, in the propagating solutions. It is important to note here that the background gauge field profile comes from the finite temperature field theory, which is formulated in the Euclidean space. To calculate the reflection and the transmission coefficients (or to study propagation of quarks, in general), we need to solve Dirac equation in the Minkowski space.

We start with the Dirac equation in the Euclidean space, with the spatial dependence of A_0 calculated from the Z(3) wall profile as mentioned above. Then we do the analytic continuation of the full equation to the Minkowski space and use the resulting equation to calculate the reflection and transmission coefficients. We should mention here that it may seem puzzling that we are extracting information about colored objects (i.e. A_0) starting with a colorless object, the Polyakov loop. However, as we will explain later in Sec. V, starting with a given profile of $L(x)$, one does not get unique solution for $A_0(x)$ and the ambiguity about color information manifests itself in the form of a set of solutions of A_0.

We will use the effective model for the Polyakov loop as proposed by Pisarski [12]. The Lagrangian density has the form

$$\mathcal{L} = \frac{N}{g^2}|\partial_\mu L|^2 T^2 - V(L). \tag{4}$$

$N = 3$ for our case (i.e. QCD). T^2 is multiplied with the first term to give the correct dimensions to the kinetic term. $V(L)$ is the potential term that has the form

$$V(L) = \left(-\frac{b_2}{2}|L|^2 - \frac{b_3}{6}(L^3 + (L^*)^3\right) + \frac{1}{4}(|L|^2)^2)b_4 T^4. \tag{5}$$

The cubic term in $L(\vec{x})$ in the above potential, when written in terms of $L(\vec{x}) = |L(x)|e^{i\theta}$, gives rise to $\cos(3\theta)$ term that leads to three degenerate $Z(3)$ vacua when $L(\vec{x}) \neq 0$ (i.e. when $T > T_c$). The coefficients b_2, b_3 and b_4, in the potential, are fixed in Refs. [18–20] by comparing with lattice results for the pressure and energy density for pure SU(3) gauge theory [21,22]. b_2 is given by $b_2 = (1 - 1.11/x)(1 + 0.265/x)^2(1 + 0.300/x)^3 - 0.478$, where $x = T/T_c$ with $T_c \sim 182$ MeV. The other parameters are $b_3 = 2.0$ and $b_4 = 0.6061 \times 47.5/16$ (the factor 47.5/16 for b_4 is to account for the additional quark degrees of freedom compared to pure SU(3) case). With the above values, $L(\vec{x}) \to y = b_3/2 + \frac{1}{2} \times \sqrt{b_3^2 + 4b_2(T = \infty)}$ as $T \to \infty$. $L(\vec{x})$ and other quantities are normalized as follows:

$$L(\vec{x}) \to L(\vec{x})/y, \quad b_2 \to b_2/y^2, \quad b_3 \to b_3/y, \quad b_4 \to b_4 y^4, \tag{6}$$

so that $L(\vec{x}) \to 1$ as $T \to \infty$. The normalized quantities are then used in Eq. (5), which is then used to calculate the $L(\vec{x})$ profile using energy minimization, see Ref. [4] for details. Figure 1 shows the plot of $|L(\vec{x})|$ for the interface between two different vacua (in the absence of quarks all the three interfaces have same profile for $|L(\vec{x})|$). We mention that the surface tension σ of the Z(3) walls was estimated in Ref. [6] for the above effective potential and it was found that $\sigma = 0.34$, 2.62, and 7 GeV/fm^2 for $T =$ 200, 300, and 400 MeV, respectively. There have been lattice studies of Z(3) wall tension. In Ref. [23] the surface tension was found to be $\sigma(T_c) = 0.17T_c^3$. With $T_c =$ 182 MeV the $T = 200$ result for σ in Ref. [6] is larger by almost factor 10 than the lattice result of Ref. [23]. However, the values of σ for larger temperatures, $T = 300$ and 400 MeV are in reasonable agreement with the analytical estimates [24] (which give $\sigma = \frac{4(N-1)\pi^2 T^3}{3\sqrt{3g}}$ for large temperatures).

The energy minimization program gives the full profile for $L(\vec{x})$ which is then used for calculating $A_0(\vec{x})$ as described in the next section. (As we mentioned in the Introduction, we will also consider another form of effective potential as provided by Fukushima [13] in Sec. IV.)

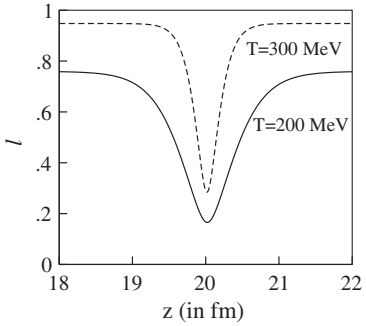

FIG. 1. Variation of $|L(\vec{x})|$ between different $Z(3)$ vacua for $T = 200$ MeV and $T = 300$ MeV respectively, as a function of z. Note that at higher temperature, the wall thickness is smaller, as expected.

III. OBTAINING A_0 PROFILE

In this section we calculate the A_0 profile form $L(\vec{x})$ profile by inverting Eq. (1). As in Ref. [10] we choose A_0 to be of the form

$$A_0 = \frac{2\pi T}{g}(a\lambda_3 + b\lambda_8), \tag{7}$$

where g is the coupling constant and T is the temperature, while λ_3 and λ_8 are the diagonal Gell-Mann matrices. Coefficients a and b depend only on spatial coordinates. The advantage of taking this gauge choice is that we are dealing with the eigenvalues of the matrices that are invariant under gauge transformation.

We take A_0 to be independent of τ. This is for simplicity. Further, it can be justified in the high temperature limit due to periodic boundary conditions on A_0 in the (Euclidean) time direction in the imaginary time formalism being used here for finite temperature field theory.

Substituting Eq. (7) in Eq. (1), we get

$$3L(x) = \exp(i\alpha) + \exp(i\beta) + \exp(i\gamma), \tag{8}$$

where $\alpha = 2\pi(\frac{a}{3} + \frac{b}{2})$, $\beta = 2\pi(\frac{a}{3} - \frac{b}{2})$ and $\gamma = 2\pi(\frac{-2a}{3})$. On comparing the real and imaginary part of Eq. (8), we get

$$\cos(\alpha) + \cos(\beta) + \cos(\gamma) = 3|L|\cos(\theta), \tag{9a}$$

$$\sin(\alpha) + \sin(\beta) + \sin(\gamma) = 3|L|\sin(\theta). \tag{9b}$$

Here θ is defined by writing $L(x) = |L(x)|e^{i\theta}$. In Eq. (1), A_0 appears in the phase, so any increment in the phase by a factor of type $2\pi n$ will result in the same value of $L(\vec{x})$. We first consider the above equations for $L = 1$ vacuum. Note that $|L| < 1$ for finite temperatures. However, we will keep referring to the three Z(3) vacua as $L = 1, Z, Z^2$. The solutions are a set of ordered pairs $(a, b)_{L=1}$. These different solution sets reflect $2\pi n$ ambiguity in A_0. Similarly, we find the solution sets $(a, b)_{L=Z}$ corresponding to the $L = Z = \exp(i2\pi/3)$ vacuum. One now needs to find the appropriate values of (a, b) for the entire profile of $L(x)$ interpolating between these two vacua. One ambiguity in this is obvious. It may appear that any of the sets $(a, b)_{L=1}$ could be matched to any of the sets $(a, b)_{L=Z}$ as all sets for a given vacua are equivalent. However, this could lead to different A_0 profiles in between, which in turn would lead to different reflection and transmission coefficients. This problem is resolved when we realize that the variation of A_0 should be smooth across the domain wall. Thus, we can simply start with any one pair $(a, b)_{L=1}$, and set it as the initial condition for the generation of the profile of A_0 as one traverses the wall starting from the $L = 1$ vacuum to the $L = \exp(i2\pi/3)$ vacuum. We only require that a and b vary smoothly as the profile of $L(x)$ changes smoothly across the wall. It will then automatically lead to the appropriate values of $(a, b)_{L=Z}$ as the $L = Z$ vacuum is approached.

For the results shown here we had taken the initial values of $(a, b) = (-1.5, -1.0)$ for the $L = 1$ vacuum (in a region far left to the interface). As one approaches the interface, say, along the z axis, a new value of $L(x)$ is selected from the profile of $L(x)$ (calculated from the energy minimization program). We then take small range of values near the original $(a, b) = (-1.5, -1.0)$, and $L(z)$ was then calculated for all these values. Those values of a and b were selected for which the error between the calculated L and L obtained by energy minimization was minimum. The process was then repeated for each value of z to obtain the a, b values. A comparison between the calculated $|L|$ profile and the one obtained by energy minimization is given in Fig. 2(a). It clearly shows that this technique works well. Figure 2(b) shows profile of parameters a and b across the domain wall.

The calculated a, b were then used to calculate A_0 using Eq (7). The A_0 profile thus obtained is reasonably well fitted to the function $A_0(x) = p\tanh(qx + r) + s$ using

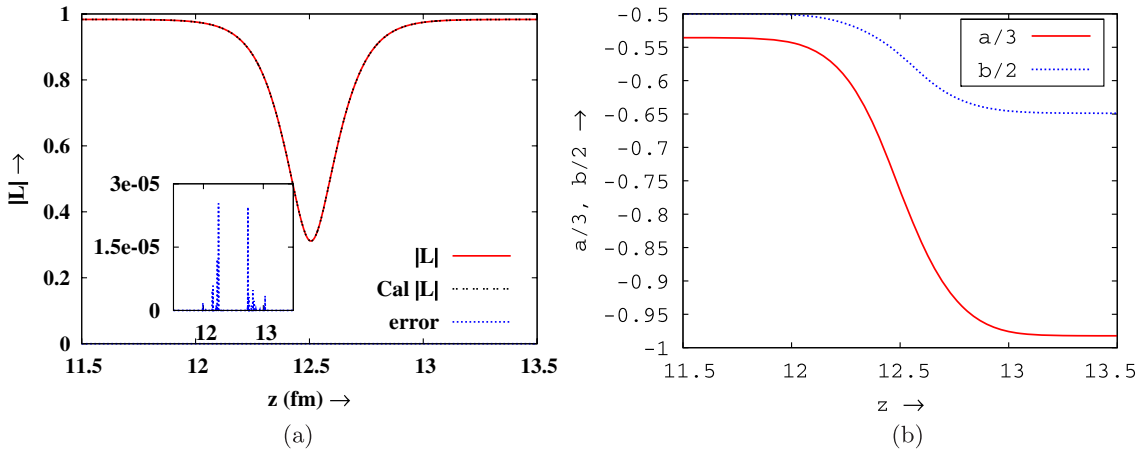

(a) (b)

FIG. 2 (color online). Left: plot of calculated $|L|$ and the one obtained from minimizing the energy. The inset figure shows the deviation between the two profiles. Right: variation of a and b between the regions $L(\vec{x}) = 1$ and $L(\vec{x}) = e^{i2\pi/3}$. Initial point is $(-1.5, -1.0)$.

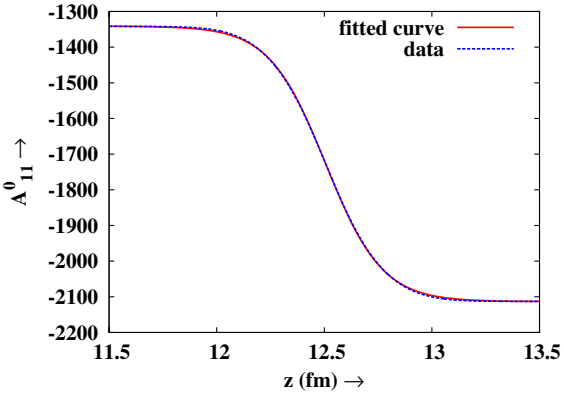

FIG. 3 (color online). Plot of calculated A_0 and the fitted profile ($A_0(x) = p\tanh(qx + r) + s$). The parameters have values $p = -378.27$, $q = 7.950\,01$, $r = -49.7141$, $s = -1692.48$. Only (1, 1) component of A_0 is plotted. The other components also have similar fit.

GNUPLOT. The calculated A_0 profile and fitted A_0 profile are plotted in Fig. 3.

IV. CALCULATION OF A_0 PROFILE FOR A DIFFERENT EFFECTIVE POTENTIAL

We now address the issue of the uncertainties in the determination of the A_0 profile depending on the choice of the specific form of the effective potential. Other parametrizations of the effective potential for the Polyakov loop have been given in the literature, e.g. in Refs. [13,14], and we will repeat the calculations of the previous section for the effective potential of the Polyakov loop as provided by Fukushima [13]. For spatially varying L configurations, we will continue to use the derivative terms as in Eq. (4) with general dimensional considerations (with suitable normalization of L). The effective potential for Ref. [13] has the following form:

$$V[L]/T^4 = -2(d-1)e^{-\sigma a/T}|\mathrm{Tr}L|^2 - \ln[-|\mathrm{Tr}L|^4 + 8\mathrm{Re}(\mathrm{Tr}L)^3 - 18|\mathrm{Tr}L|^2 + 27]. \quad (10)$$

$\sigma = (425\ \mathrm{MeV})^2$ is the string tension and $2(d-1)e^{-\sigma a/T_d} = 0.5153$ with $T_d = 270$ MeV is taken as the transition temperature by choosing the lattice spacing $a = (272\ \mathrm{MeV})^{-1}$. Note that for consistency with the notations of Ref.[13], we will use T_d and T_c interchangeably, both meaning the deconfinement transition temperature. L is the Polyakov loop but without the normalizing factor of $N_c(= 3)$. (Thus, using with Eq. (4) we rewrite the above effective potential in terms of the normalized Polyakov loop. Henceforth by L even for the above equation we will mean this normalized Polyakov loop). It has been argued by Schaefer *et al.* [25] that the transition temperature has to be tuned depending on the number of quark flavors N_f (and also the value of the baryon-chemical potential). In Ref. [25], the value of $T_d = 270$ MeV corresponds to the pure SU(3) case with $N_f = 0$. In Sec. II we have used the effective potential where the coefficient b_4 is suitably normalized for the case of 3 flavors, $N_f = 3$. For the case of $N_f = 3$, the value of transition temperature from Ref. [25] is $T_d = 178$ MeV. Thus, we will use this value of T_d for the effective potential in Eq. (10).

The effective potential in Eq. (10) is of qualitatively different nature than the one given in Eq. (5). For small values of L the two forms will be similar as one can see by the expansion of the logarithmic term in the above equation. However, for $|L|$ approaching 1 the two potentials are dramatically different. $V[l]$ in Eq. (10) diverges at this limiting value thereby constraining $|L|$ within value 1. There is no such constraint in Eq. (5). Even the shape of $V[L]$ is very different away from the origin, especially near the three $Z(3)$ vacua. It is thus reasonable to expect that the resulting profile of $Z(3)$ wall and resulting A_0 profile (using the calculations of previous sections) for Eq. (10) may be quite different from the ones obtained in Sec. III for Eq. (5).

With diverging $V[L]$ at $|L| = 1$ in Eq. (10), and due to its nontrivial shape near the $Z(3)$ vacua, the application of the technique of Ref. [4] for the determination of L profile between two Z(3) vacua is much more complicated here. Especially nontrivial is the choice of initial ansatz for the wall profile which is used for the energy minimization program. In Ref. [4], the initial profile was taken to linearly interpolate between the two Z(3) vacua as a function of spatial coordinate z. This choice simply does not work for Eq. (10) due to the fact that $V[L]$ diverges at $|L| = 1$ and linear interpolation takes it outside this bound. For this we chose the initial trial profile to consist of two parts, one linearly decreasing (with z) to $L = 0$ along $\theta = 0$ from the vacuum value and join this with the second part linearly increasing (with z) along $\theta = 2\pi/3$ to the second vacuum value. This keeps the initial profile within the allowed region of $V[L]$ in Eq. (10).

A second complication arises with the algorithm of energy minimization itself. In Ref. [4] correct L profile was obtained from the initial trial profile by fluctuating the value of L at each lattice point and determining the acceptable fluctuation which lowers the energy (with suitable overshoot criterion, etc. as described in detail in Ref. [4]). However, with Eq. (10), fluctuations of L can take it out of the allowed region of $V[L]$. For this, we skip those fluctuations which take L outside the allowed region. With these modification in the procedure, we were able to determine the profile of the Z(3) wall and associated A_0 profile. In Sec. III we had calculated the profiles for temperature $T = 400$ MeV [with $T_c = 182$ MeV for the effective potential in Eq. (5)]. For the sake of comparison with that case, for $V[L]$ in Eq. (10) with $T_c = 178$ MeV [25], we calculate the profiles for $T = 391$ MeV which is close enough to the value $T = 400$ MeV, and has the same value for T/T_c.

Figure 4(a) shows the wall profile of $|L|$ for $V[L]$ in Eq. (10) [again, with normalized L]. The profile is almost the same as the one shown in Fig. 2(a). We mention here that for Fig. 4(a) we have used the same value of the coefficient of the first $|\mathrm{Tr}L|^2$ term in Eq. (10) as with $T_d = 270$ MeV (by suitably changing the values of string tension, etc.). This is so that the shape of the barrier near the confining vacuum remains unaffected (which determines the first order nature of the transition). In any case, the overall features of the profile of the wall, such as its width and height, should depend more on the temperature scale rather than on the shape of the barrier for the confining vacuum. To check this, we also calculate the wall profile of $|L|$ for Eq. (10), but now with the value of $T_d = 270$ MeV and $T = 400$ MeV. The comparison of the two profiles is shown in Fig. 4(b). We see that the two profiles are very close to each other confirming above arguments.

We recalculate the plots of a and b for the case with $T = 391$ MeV (with $T_d = 178$ MeV). The resulting plots are shown in Fig. 5(a) which are seen to be very similar to those on Fig. 2(b). Finally, the profile of A^0_{11} in Fig. 5(b) is also very close to the one in Fig. 3. Note that though overall all the plots in Figs. 4 and 5 are very close to the corresponding plots in Figs. 2 and 3, there is one clear difference. The profiles in Figs. 4 and 5 have somewhat sharper variations from their asymptotic values compared to the case in Figs. 2 and 3. This originates from the qualitatively different shapes of the two potentials in Eqs. (5) and (10) near the region of Z(3) vacua, and in that sense characterizes the difference in the two potentials.

These results are quite remarkable. Even though the two effective potentials Eq. (5) and (10) (from Refs. [12,13]) are of qualitatively different shapes, the resulting wall profile and A_0 profile are almost the same. As we mentioned above, for small values of L the two effective potentials will have similar forms, which are fitted with the lattice data. Our results thus point out that the profile of L (and consequently, the profile of A^0) are primarily determined by the small L region of the effective potentials. This is likely to happen if the variations near the $Z(3)$ vacua

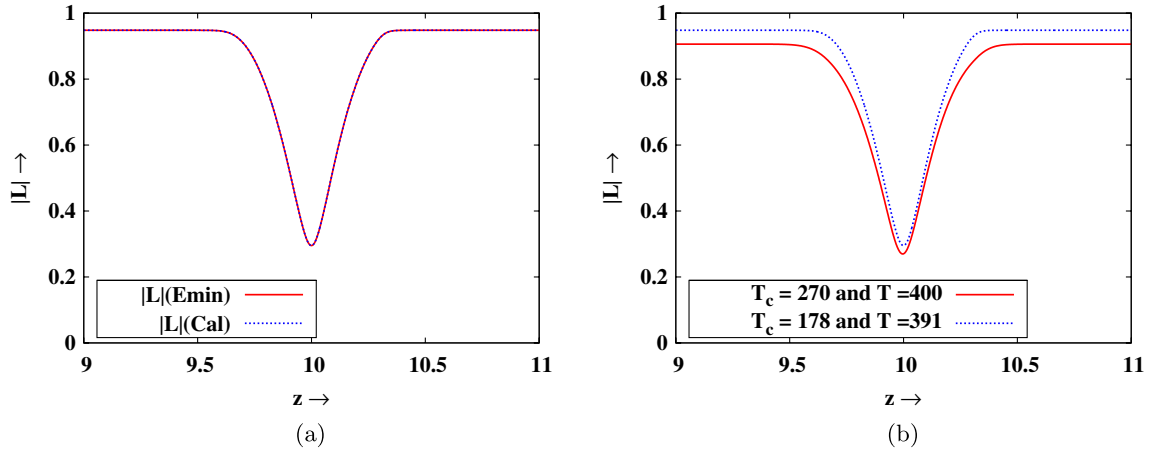

FIG. 4 (color online). (a) Plot of the profile of $|L|$ corresponding to the effective potential in Eq. (10). (b) Comparison of the profiles of $|L|$ for different choices of T_d in Eq. (10).

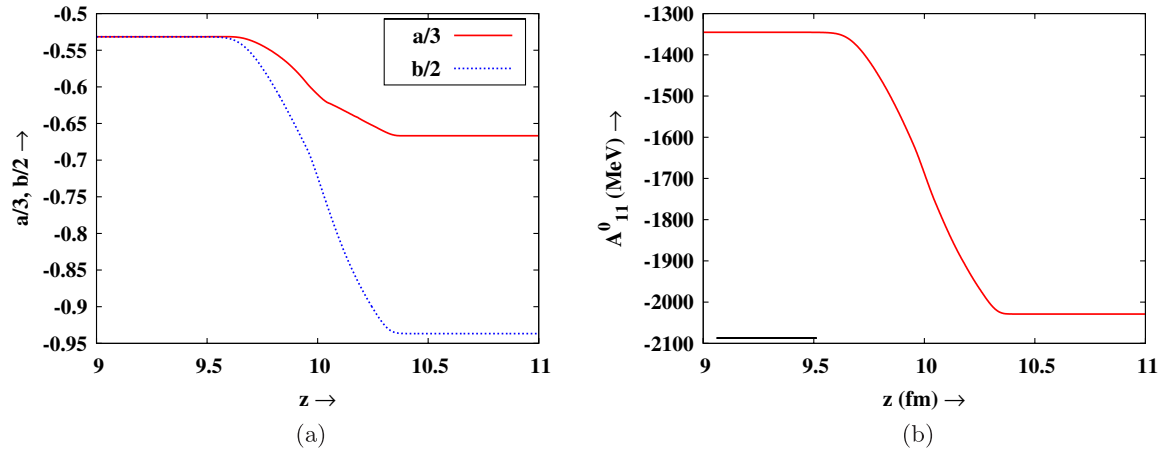

FIG. 5 (color online). (a) Plot of calculated values of a and b for the $|L|$ profile of Fig. 4(a). (b) corresponding plot of A_0.

are primarily in the magnitude of L and not in its phase. The robustness of our results against different choices of the effective potentials gives us confidence in the use of our procedure to calculate the reflection of quark and antiquarks from the Z(3) interfaces. Since the A_0 profiles of Figs. 3 and 5 are almost the same, the resulting values of reflection coefficients for quarks/antiquarks will also be very similar. In the rest of the analysis in the paper, we will use the effective potential as given in Eq. (5).

V. CALCULATING REFLECTION AND TRANSMISSION COEFFICIENTS

To calculate the reflection and transmission coefficient, we need the solutions of Dirac equation in the Minkowski space. We start with the Dirac equation in the two-dimensional Euclidean space

$$[i\gamma_e^0\partial_0\delta^{jk} - g\gamma_e^0 A_0^{jk}(z) + (i\gamma_e^3\partial_3 + m)\delta^{jk}]\psi_k = 0, \quad (11)$$

where $\gamma_e^0 \equiv i\gamma^0$ and $\gamma_e^3 \equiv \gamma^3$ are the Euclidean-Dirac matrices. ∂_0 denotes ∂/∂_τ with $\tau = it$ being the Euclidean time. j, k denote color indices. We now analytically continue Eq. (11) to the Minkowski space to get

$$[i\gamma^0\partial_0\delta^{jk} + g\gamma^0 A_0^{jk}(z) + (i\gamma^3\partial_3 + m)\delta^{jk}]\psi_k = 0, \quad (12)$$

where now ∂_0 denotes $\partial/\partial t$ in the Minkowski space. Note that the A_0 in Eq. (12), which is in the Minkowski space, is fundamentally different from the A_0 in Eq. (11) which is in the Euclidean space. However, it is the *same domain wall profile* (i.e. the same A_0 dependence on z) that appears in both the cases, which is what is needed for the calculation of reflection and transmission coefficients. For a wave function with time dependence $\psi(x)e^{-iEt}$, Eq. (12) reduces to

$$[\gamma^0\gamma^3\partial_3\delta^{jk} + \gamma^0 m\delta^{jk}]\psi_k(x) = (E - V_0(z))\psi_k(x), \quad (13)$$

where $V(z) = -gA_0^{jk}(z)$ is the potential as seen by the incoming fermion. We do not have any analytic way to calculate the reflection and transmission coefficients for a general smooth potential, so we follow a numerical approach. Kalotas and Lee [26] have discussed a numerical technique to solve the Schrödinger equation, approximating a general smoothly varying (in space) potential in terms of a sequence of step functions. We follow their approach and apply their technique for solving the Dirac equation [Eq. (13)]. We approximate the actual potential by n step potentials in a series, each of equal width w as shown in Fig. 6. Let ψ_j be the wave function for the jth bin and the height of potential be V_j. (We consider a spin up wave function and restrict to a no-spin-flip situation.) The height of the jth step potential is taken to be the mean value of $V(L + jw)$ and $V(L + (j + 1)w)$, i.e.

$$V_j = \frac{[V(L + jw) + V(L + (j + 1)w)]}{2}. \quad (14)$$

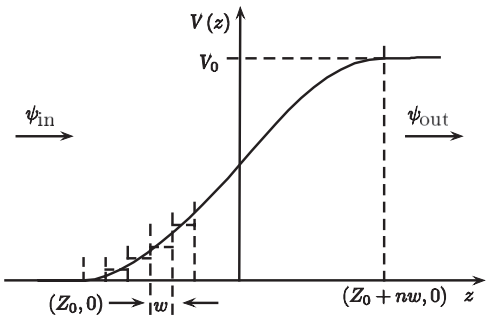

FIG. 6. Potential ($V(z)$) approximated by a sequence of n step potentials, each of width w.

We now apply boundary conditions at j^{th} step i.e. at $z = L + jw$. This gives us a set of two equations, which when iteratively solved give

$$\begin{pmatrix} A_{\text{in}} \\ B_{\text{in}} \end{pmatrix} = M^{-1}(L, k_{\text{in}}) \times M(L, k_1) \times \ldots M^{-1}(L + nw, k_n) \times M(L + nw, k_{\text{out}}) \begin{pmatrix} A_{\text{out}} \\ 0 \end{pmatrix} \quad (15a)$$

$$M(L + jw, k_q) = \begin{pmatrix} e^{ik_q(L+jw)} & e^{-ik_q(L+jw)} \\ \frac{e^{ik_q(L+jw)}k_q}{E_q+m} & -\frac{e^{-ik_q(L+jw)}k_q}{E_q+m} \end{pmatrix} \quad (15b)$$

with $k_q = \sqrt{E_q^2 - m^2}$, and $E_q = E - V_q$. (Here no left moving wave is allowed in the region far right of the interface.) The reflection and transmission coefficients are then given by

$$R \equiv \left|\frac{J_{\text{ref}}}{J_{\text{in}}}\right| = \left|\frac{B_{\text{in}}}{A_{\text{in}}}\right| \quad (16a)$$

$$T \equiv \left|\frac{J_{\text{trans}}}{J_{\text{in}}}\right| = \left|\frac{A_{\text{out}}}{A_{\text{in}}}\right| \times r, \quad (16b)$$

$$\text{where } r = \left(\frac{k_{\text{out}}}{k_{\text{in}}}\right)\left(\frac{E + m}{E - V_{max} + m}\right). \quad (16c)$$

Here, $k_{\text{in}} = \sqrt{E^2 - m^2}$ and $k_{\text{out}} = \sqrt{(E - V_0)^2 - m^2}$.

VI. RESULTS

We first calculated the reflection and transmission coefficients by assuming the A_0 profile to be a step function rather than a smooth one, with the height of the step function being the same as that of the interface in Fig. 6. In this approximation one can calculate the reflection and transmission coefficients analytically. For antiquarks the reflection and transmission coefficients are obtained by changing $g \to -g$, as antiquarks are in $\bar{3}$ representation of $SU(3)$. We have chosen the energies of the particles such that $E > V + m$, so as to avoid the Klein paradox regime. Note that if $E < V$ (but $V - E < m$ so that one is away

TABLE I. Table for the reflection coefficients for various quarks in the step function approximation. Reflection is higher for heavier quarks.

	u	d	s	c
E (GeV)	3.0	3.0	3.0	3.0
m (MeV)	2.5	5.0	100	1270
R_q	1.73×10^{-7}	6.76×10^{-7}	2.8×10^{-4}	0.14
$R_{\bar{q}}$	1.92×10^{-8}	7.55×10^{-8}	3.2×10^{-5}	6.5×10^{-3}

from Klein paradox situation), then the reflection coefficient for quarks is 1 (repulsive potential) but for antiquarks reflection coefficient will be very small with $-V$ providing the attractive potential. This will provide the most dramatic difference between the reflection of quarks and that of antiquarks from Z(3) walls. However, for the relevant energies of quarks/antiquarks at RHICE, we discuss in detail the case with $E > V + m$.

The results for different quarks and antiquarks (with $E = 3.0$ GeV for each case) are given in Table I. It is clear that quarks have different reflection coefficients than their CP conjugates. Also, the effect is significantly higher for the heavier quarks (for example, charm quark).

We now calculate the reflection coefficient for charm quark using the exact potential. The product of the matrices in Eq. (15) were calculated by a FORTRAN code and also by using MATHEMATICA. Equation (16) was then used to calculate the reflection coefficient. At $E = 3$ GeV, we get $R = 0.0011$ for c quark while for $\bar{c}$ the result is $R = 5.24 \times 10^{-10}$. As an additional check on the results (for the smooth profile), we consider shrinking of the profile of A_0 in z direction, and compared the reflection coefficient (for the c quark with 3 GeV energy) with the step potential result. The results are summarized in Table II. We see that the numerical results approach the analytical results of the step function as A_0 profile is shrunk along z to better approximate a step function. This gives us the confidence that our numerical technique of solving the Dirac equation is reliable.

It is clear that if one considers the situation of quarks/antiquarks coming from right in Fig. 6 (i.e. approaching the domain wall from the side with $L = Z$) then antiquarks will have larger reflection coefficients while quarks will have smaller reflection coefficients. Also we should mention that Eq. (13) is solved by using one component of A_0 profile (A_0^{11} in this case), which gives us the reflection coefficient for one particular color (say red). The reflection coefficient for other colors will remain the same when the $SU(3)_c$ gauge transformation is applied on the quark as well as on the vector potential. However, there is still an ambiguity of starting with different initial sets (a, b) (say in the $L = 1$ vacuum). Different sets lead to different profiles for (a, b) across the domain wall, thus A_0 profile depends on the initial condition (which, in turn, will lead to different reflection coefficients for a quark of a given color).

TABLE II. Table for the reflection coefficients for c quark, with 3 GeV energy, when the profile is shrunk. Results approach the step potential as the profile gets narrower.

Shrinking factor	Reflection coeff.
No shrinking	0.0011
0.5	0.017
0.05	0.119
0.005	0.123
Step potential	0.140

As we mentioned earlier, this ambiguity is reasonable in view of the fact that we are extracting information about a colored object (A_0) starting from a colorless variable $L(x)$. Thus there is no reason to expect unique solution for A_0 starting from a given $L(x)$ profile, even in the diagonal gauge where A_0 is determined in terms of real (a, b).

For several sets of values of (a, b) we have checked that different choices of (a, b) are related to each other by color transformation. We can explain it in the following way: Say we start with (a_1, b_1) for $L = 1$ vacuum and calculate the profile $(a(x), b(x))$ leading to profile of A_0. Now A_0^{11}, A_0^{22}, A_0^{33} all have different profiles and correspond, respectively, to scattering of red, blue, and green quarks, respectively, from the given domain wall profile. Now if we start with a different set (a_2, b_2) and calculate the profile of A_0 then we find (for example) that new A_0^{11} is the same as old A_0^{22} (where one started with (a_1, b_1)) and new A_0^{22} is the same as old A_0^{11}. This means that (a_2, b_2) set gives the same reflection for the blue quark as (a_1, b_1) gives for the red quark. Thus we say that our different choices of (a, b) amount to considering quarks of different colors for a given domain wall profile. Or, equivalently, for the scattering of a fixed color (say red) quark, different sets (a, b) lead to domain wall profiles carrying different color information. (We should mention that this holds for many sets (a, b) we have checked. However, we do not have a general proof that this should be true for all sets, though it looks very likely in view of the above arguments).

For example, if we start with $(a', b') = (a, -b)$, i.e. with $(-1.5, 1)$, then Eq. (7) tells us that $A_0'^{11} = A_0^{22}$ and $A_0'^{22} = A_0^{11}$. See Fig. 7 for the corresponding profiles of (a,b). In color space A_0 is diagonal with elements $(A_0^{11}, A_0^{22}, A_0^{33})$, and it acts on the color triplet $(r, b, g)^T$. So, A_0^{11} acting on $(1, 0, 0)^T$ is same as $A_0'^{22}$ acting on $(0, 1, 0)^T$ which is same as making different choices in color space.

So, the ambiguity related to various (a, b) profiles or, equivalently, corresponding A_0 profiles, seems to be the artifact of the ambiguity of making a color choice for the domain wall profile in terms of A_0, starting from the domain wall profile in terms of $L(x)$.

This raises an important question: whether we should be dealing with colored domain wall profile (given in terms of A_0 profile) at all, or should we restrict to colorless objects

like $L(x)$ (which is what was done in our earlier works, see Refs. [4,6])? After all, the effective potential which we use is given in terms of $L(x)$. Here we think that there is no reason to restrict to colorless objects. We are dealing with the QGP phase and there is no requirement of physical observables to be color singlets. If we were dealing with the confining phase then we had obligation of dealing with colorless objects as physical observables. For the QGP phase, it should make perfect sense to think of the domain wall profile as having color properties as it arises from the A_0 profile. Of course it is possible that the actual domain wall profile is color insensitive, and quarks of all colors have the same reflection coefficient from a given wall. But it is also possible that the wall is colored and a given wall has a different reflection for quarks of different colors. The only requirement of gauge invariance is that when color gauge transformations are done on the $A_0(x)$ profile as well as on quarks, then the numbers should not change, which is obviously true with the Dirac equation we are using.

VII. DISCUSSION

This *CP* violation will have interesting observable consequences for the relativistic heavy ion collision experiments at the RHIC and at the LHC. If QGP is formed in these experiments (and there are strong indications of that), then various $Z(3)$ domains will inevitably be formed, leading to the formation of Z(3) walls. (We mention that the QGP strings [4] which also necessarily form during transition to QGP phase should also lead to spontaneous *CP* violation. Its effects on quark/antiquarks scattering, or possible localization on the QGP strings needs to be explored). As these domain walls move/collapse, quarks/antiquarks will get reflected/transmitted differently from these domain walls leading to the segregation of quarks and antiquarks. The concentration of quarks (or antiquarks, depending on the collapsing vacuum) will grow in different regions of the QGP. As the effects would be stronger for heavier quarks (Table I), this should lead to enhancement of strange and charmed baryons along with the suppression in the yield of corresponding mesons (such as J/ψ).

Detailed exploration of the formation and evolution of Z(3) walls and QGP strings in the context of RHICE has been carried out in Ref. [5]. These simulations show that in the typical region of QGP formed in RHICE, one expects several Z(3) domain walls to form, their numbers ranging from 1 to 4, 5. The walls may extend throughout the QGP region with size of order 10 fm. There are closed domain walls formed with initial size of about 5–8 fm. The velocities of these walls was also estimated in Ref. [5] and were found to range from 0.5 to 0.8. For a detailed discussion of the properties of Z(3) wall and QGP string networks expected in RHICE, see Ref. [5]. These results about the sizes and numbers of Z(3) walls and QGP strings are very important. This is because one should realize that in a very large sized QGP region, as in the early Universe, for every domain wall connecting $\theta = 0$ and $\theta = 2\pi/3$ vacua, there will be one connecting $\theta = 0$ and $\theta = 4\pi/3$ vacua. These walls are conjugate of each other and the reflection of a quark from the first wall is identical to the reflection of an antiquark from the second wall. These two walls are strictly degenerate, even in the presence of explicit symmetry breaking effects from dynamical quarks. Thus, on the average there will not be any bias for quarks and antiquarks as they scatter from a network of Z(3) walls.

This is, however, not true for a small QGP region as produced in RHICE. As the number of Z(3) walls produced in such a small region is of order one [5], there may be a net effect for the concentration of baryon number, or for antibaryon, in each event. This can be revealed by event-by-event analysis. Even statistically, for a large number of events, one can calculate the variance of baryon number density, and spontaneous *CP* violation from Z(3) walls may be detected. For a given event also, segregation of baryons and antibaryons will occur over large distances of order several fm as indicated by the typical wall size and separation [5].

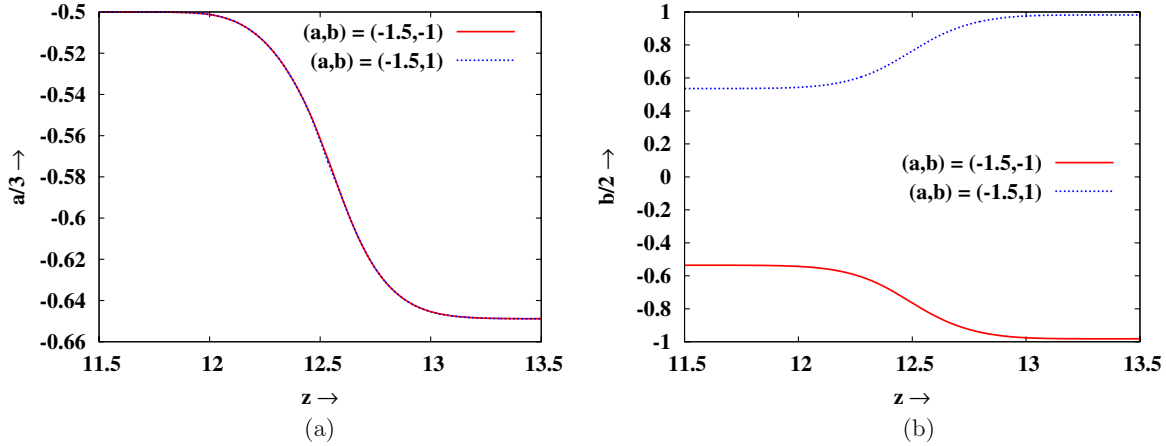

FIG. 7 (color online). Left: variation of a for different initial values of a, b. As a is unchanged, its profile is unaffected. Right: variation of b for different initial values for b. As b changes sign in the initial values, its profile also changes.

This CP violation can also be very important in the context of the early Universe where it can have interesting implications for generation of baryon inhomogeneities. As collapsing domain walls preferentially sweep quarks (or antiquarks), segregation of quarks and antiquarks will occur. One can then discuss the formation of baryonic (or antibaryonic) lumps. These baryon inhomogeneities can be of large magnitude, with large separations in the context of certain low energy inflationary models [6], (but now with CP violation incorporated). We will present a detailed study of this in a future work.

Another important consequence will be on the P_t spectra of hadrons. The quarks/antiquarks with high momenta will undergo nontrivial scattering from these Z(3) walls. As $Z(3)$ walls collapse, some get transmitted while others are reflected back. For $Z(3)$ walls forming closed, collapsing, structures, the quarks suffer multiple reflections inside the wall, resulting in an increment in their transverse momenta. This process continues until the walls either melt away or collapse completely. So the final transverse momentum of some quarks may be reasonably enhanced before they escape. One can then use a specific model (such as the recombination/coalescence model) to study the P_t spectra of final state hadrons, which should show an increase in the yield of hadrons at high P_t. This has been discussed in Ref. [27], however, no account of CP violation was considered in that work. In the presence of CP violation, the modified P_T spectra will be different for quarks and for antiquarks. We plan to carry out these analyses in a future work.

The most important limitation of our analysis is the absence of quark effects. Dynamical quarks will lead to lifting of degeneracy between different Z(3) vacua, making $L = 1$ vacuum as the true vacuum as discussed in Refs. [12,18–20]. The one-loop corrections from dynamical quarks have also been discussed in Refs. [28–31]. As we mentioned, recent lattice studies [9] have provided evidence for the existence of such metastable Z(3) vacua. Our analysis above of calculation of A_0 profile and calculation of reflection coefficients for quarks and antiquarks can be straightforwardly applied for this nondegenerate case and work is underway on this. Apart from affecting the numbers (for reflection coefficients), its most important effect will be on the evolution of Z(3) wall and QGP string network, (see Ref. [32] for a detailed simulation study of these aspects). However, for the case of RHICE, due to small length (and time) scales involved, the dynamics of Z (3) walls is likely to remain dominated by the surface tension effects with the difference in pressure between different vacua not playing dominant role for such length scales). Thus the above mentioned features of effects on hadron spectra due to CP violation may remain qualitatively true for RHICE.

However, for the Universe the entire issue of formation and evolution of Z(3) walls crucially depends on the importance of quark effects. Some discussion of this has been provided in [6] and we plan to investigate these issues in future in detail. The most important issue will be to see whether the spontaneous violation of CP discussed here can lead to a net separation of baryons and antibaryons in the Universe which will have observational consequences (e.g. from the strongly constrained nucleosynthesis, which can be used to constrain various parameters of the model).

ACKNOWLEDGMENTS

We are extremely thankful to C. Korthals Altes, A. P. Balachandran, B. Rai, P. Agrawal, S. Digal, and R. Ray for their valuable comments. We would also like to thank U. Shankar Gupta, A. P. Mishra, P. S. Saumia, R. Mohapatra, P. Bagchi, and V. Tiwari for fruitful discussions.

[1] T. Bhattacharya, A. Gocksch, C. Korthals Altes, and R. D. Pisarski, Nucl. Phys. **B383**, 497 (1992).
[2] S. T. West and J. F. Wheater, Nucl. Phys. **B486**, 261 (1997).
[3] J. Boorstein and D. Kutasov, Phys. Rev. D **51**, 7111 (1995).
[4] B. Layek, A. P. Mishra, and A. M. Srivastava, Phys. Rev. D **71**, 074015 (2005).
[5] U. S. Gupta, R. K. Mohapatra, A. M. Srivastava, and V. K. Tiwari, Phys. Rev. D **82**, 074020 (2010).
[6] B. Layek, A. P. Mishra, A. M. Srivastava, and V. K. Tiwari, Phys. Rev. D **73**, 103514 (2006).
[7] A. V. Smilga, Ann. Phys. (N.Y.) **234**, 1 (1994).
[8] V. M. Belyaev, I. I. Kogan, G. W. Semenoff, and N. Weiss, Phys. Lett. B **277**, 331 (1992).
[9] M. Deka, S. Digal, and A. P. Mishra, arXiv:1009.0739.
[10] C. P. Korthals Altes and N. J. Watson, Phys. Rev. Lett. **75**, 2799 (1995).
[11] C. P. Korthals Altes, AIP Conf. Proc. **272**, 1443 (1992).
[12] R. D. Pisarski, Phys. Rev. D **62**, 111501 (2000).
[13] K. Fukushima, Phys. Lett. B **591**, 277 (2004).
[14] S. Roessner, C. Ratti, and W. Weise, Phys. Rev. D **75**, 034007 (2007).
[15] A. M. Polyakov, Phys. Lett. **72B**, 477 (1978).
[16] D. J. Gross, R. D. Pisarski, and L. G. Yaffe, Rev. Mod. Phys. **53**, 43 (1981).
[17] L. D. McLerran and B. Svetitsky, Phys. Rev. D **24**, 450 (1981).
[18] A. Dumitru and R. D. Pisarski, Phys. Lett. B **504**, 282 (2001).

[19] A. Dumitru and R. D. Pisarski, Phys. Rev. D **66**, 096003 (2002).
[20] A. Dumitru and R. D. Pisarski, Nucl. Phys. **A698**, 444 (2002).
[21] G. Boyd *et al.*, Nucl. Phys. **B469**, 419 (1996).
[22] M. Okamoto *et al.* (CP-PACS Collaboration), Phys. Rev. D **60**, 094510 (1999).
[23] K. Kajantie, L. Karkkainen, and K. Rummukainen, Nucl. Phys. **B357**, 693 (1991).
[24] T. Bhattacharya, A. Gocksch, C. Korthals Altes, and R. D. Pisarski, Phys. Rev. Lett. **66**, 998 (1991).
[25] B. J. Schaefer, J. M. Pawlowski, and J. Wambach, Phys. Rev. D **76**, 074023 (2007).
[26] T. M. Kalotas and A. R. Lee, Am. J. Phys. **59**, 48 (1991).
[27] A. P. Mishra, A. M. Srivastava, and V. K. Tiwari, Indian J. Phys. B **85**, 1161 (2011).
[28] M. Ciminale, R. Gatto, N. Ippolito, G. Nardulli, and M. Ruggieri, Phys. Rev. D **77**, 054023 (2008).
[29] W.-j. Fu, Z. Zhang, and Y.-x. Liu, Phys. Rev. D **77**, 014006 (2008).
[30] P. Costa, M. Ruivo, C. de Sousa, H. Hansen, and W. Alberico, Phys. Rev. D **79**, 116003 (2009).
[31] G. Marko and Z. Szep, Phys. Rev. D **82**, 065021 (2010).
[32] U. S. Gupta, R. K. Mohapatra, A. M. Srivastava, and V. K. Tiwari, arXiv:1111.5402.